TOC Figure and Text

On the Interfacial Assembly of Anisotropic Amphiphilic Janus Particles

Alex McGlasson[1], Eva Morgenthaler[1], Laura C. Bradley[1], and Thomas P. Russell[1,2]*

[1]Department of Polymer Science and Engineering, University of Massachusetts Amherst, Amherst, Massachusetts, 01003, United States

[2]Material Science Division, Lawrence Berkeley National Laboratory, Berkeley, CA, 94720, United States

*Corresponding Author's Email: russell@mail.pse.umass.edu

TOC Text

This study focuses on the interfacial assembly mechanism of anisotropic amphiphilic Janus particles as a function of concentration, morphology, amphiphilicity, and NaOH and HCl concentration. Characterization by dynamic pendant drop tensiometry provides new insights into controlling the kinetics of Janus particle assembly and the equilibrium configuration of Janus particles at the interface.

TOC Figure

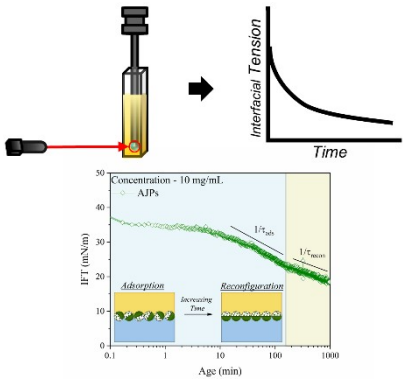

On the Interfacial Assembly of Anisotropic Amphiphilic Janus Particles

Alex McGlasson[1], Eva Morgenthaler[1], Laura C. Bradley[1], and Thomas P. Russell[1,2]*

[1]Department of Polymer Science and Engineering, University of Massachusetts Amherst, Amherst, Massachusetts, 01003, United States

[2]Material Science Division, Lawrence Berkeley National Laboratory, Berkeley, CA, 94720, United States

*Corresponding Author's Email: russell@mail.pse.umass.edu

Keywords

Janus particles, interfacial assembly, interfacial dynamics

Abstract

It has been shown both theoretically and experimentally that amphiphilic Janus particles are the most effective solid surfactants to stabilize interfaces. In most cases, the Janus particles investigated have uniform morphologies with Janus boundaries dividing the particle into halves. However, there are many examples of Janus particles where the hydrophilic and hydrophobic domains are not equally distributed. The effects of this uneven domain distribution on the mechanism and kinetics of Janus particle assembly, and final equilibrium state are not well-understood. Dynamic pendant drop tensiometry offers a means to probe both the equilibrium assembly, and the kinetics and mechanism of assembly. Here, the interfacial kinetics and assembly of spherical anisotropic Janus particles are investigated using dynamic pendant drop tensiometry. Systematic studies quantifying the time-dependent interfacial behavior as a function of Janus particle morphology, chemical composition, particle concentration, and NaOH and HCl concentration are performed. These studies shed light on the assembly mechanism of more complex Janus particle morphologies and highlight their effectiveness as interface stabilizers.

Introduction

The interface between two immiscible liquids affords an ideal platform for assembling nanomaterials that can impart functional properties to a liquid construct.[1,2] The assembly of nanomaterials at interfaces was first described in the work of Ramsden[3] and Pickering.[4] Their work showed that particulates dispersed in either phase will readily segregate to a liquid-liquid interface to reduce the interfacial energy. These findings sparked the development and use of these materials in applications such as Pickering Emulsions,[5–8] colloidosomes,[9–12] flow-through chemical reactors,[13–18] environmental remediation,[19–25] and all liquid electronics.[26–29]

The driving force for the assembly of nanomaterials at interfaces is to minimize the thermodynamic penalty that arises from the formation of an interface between two immiscible liquids. By assembling the particles at the interface of the liquids, contact between the two liquids and the interfacial energy is reduced. Koretsky and Kruglyakov derived an equation for ΔE, the change in interfacial energy (i.e. the binding energy), for a system of spherical particles with homogeneous surface chemistry,[30,31]

$$\Delta E = \pi r^2 \gamma_{ow} \left(1 - |\cos\theta|\right)^2 \quad (1)$$

where r is the particle radius, γ_{ow} is the oil-water interfacial tension, and θ is the contact angle at the three-phase contact line between the two immiscible phases and the absorbed particle. From equation (1) the reduction in interfacial energy is strongly dependent on the size of the particle and the contact angle at the three-phase contact line. As particle size increases, the binding energy increases. This makes it difficult to remove large particles from an interface once they are adsorbed. For smaller particles and nanomaterials, the binding energy is orders of magnitude lower. Consequently, nanomaterials and smaller particles can reversibly adsorb and desorb to the interface, unlike their larger counterparts. To prevent the desorption of nanomaterials from the interface a nanoparticle surfactant strategy was developed that markedly increases the binding energy of the nanomaterials to the interface.[32–34] In this strategy an electrostatically

complementary polymeric ligand is dispersed in the opposite phase of the nanomaterials. Electrostatic attraction between the nanomaterials and the ligands causes a cooperative assembly between the nanoparticles and polymeric ligands at the interface. This strategy greatly increases the binding energy of the nanomaterials, and generally results in an irreversible binding of the nanomaterials to the interface. Consequently, if the interfacial area is decreased the nanomaterials assembled at the interface will jam, locking in non-equilibrium shapes of the liquids.

While nanoparticle surfactants are effective in preventing nanomaterial desorption, the introduction of ligands in the second phase is not always ideal. An alternate strategy to increase the binding energy of nanomaterials to interfaces is to use Janus particles or materials. Janus particles are micron or nanoscale colloids with sides that are asymmetric in chemical composition, charge density, or surface properties.[35–41] For Janus particle surfactants, the asymmetry is typically such that one domain is hydrophobic, and the other is hydrophilic. This class of Janus particles are generally termed amphiphilic Janus particles.[42,43] In work done by Binks et al. it was shown that, compared to their homogeneous counterparts, Janus particles exhibited a threefold increase in their binding energy to an immiscible interface.[44] This significant increase in binding energy makes Janus particles ideal candidates for solid surfactants.

There are several techniques one can use to generate Janus particles.[45–47] Seeded emulsion polymerization (SEP), a heterogeneous polymerization method, has been adopted in numerous laboratories.[48–52] Here, a polymeric seed particle is swollen with a monomer feed and an initiator within a surfactant-stabilized seeded emulsion droplet. Upon polymerization of the monomer feed, polymerization-induced phase separation occurs producing a kinetically trapped chemically and morphologically anisotropic Janus particle.[53] The kinetically trapped morphology can be rearranged to an equilibrium phase separated morphology using solvent-assisted phase separation (SAPs).[54] In SAPs the polymer particle is swollen with an annealing solvent within a surfactant-stabilized droplet. The particles are then annealed at an elevated temperature to reach their equilibrium configuration. In addition to morphological changes, one can also introduce chemical changes to one of the domains to produce Janus particles with chemical anisotropy. Tu et al. showed that using seeded emulsion polymerization one could produce pH-responsive

amphiphilic Janus particles using acid-catalyzed hydrolysis (ACH) post-particle synthesis.[55] These Janus particles could then be used as stimuli-responsive solid surfactants which could switch their emulsion type by tuning the system pH.

The utility of SEP and other techniques for fabricating Janus particles has led to numerous experimental studies examining the interfacial behavior of Janus particles. Previous studies have focused on how varying synthetic and experimental conditions of the system can change the equilibrium interfacial behavior. Glaser et al.[56] were one of the first to experimentally confirm that amphiphilic Janus nanoparticles showed an enhanced ability to stabilize oil/water interfaces, as predicted by Binks et al.[44] Lan et al. showed that tuning the position of the Janus boundary in amphiphilic Janus particles allows one tune the properties of the resulting Pickering emulsions.[57] Park et al. showed that Janus particles exhibit attractive interactions when assembled at oil/water interfaces due to quadripolar capillary interactions.[58] However, Janus particles containing a negatively charged hemisphere overcame this attraction and exhibited repulsive interactions. It was also shown in a separate work that cylindrical Janus particles adsorb to air-water interfaces with either an end-on or a tilted configuration.[59] The particle configuration can subsequently be controlled by replacing the air with an oil phase. Razavi et al. showed that Au/SiO_2 Janus particles where the Au domain is comprised of Au nanoparticles significantly reduces the IFT of an air/water interface compared to a smooth Au cap.[60] In a separate work, it was shown that the deformation of monolayer assemblies of Au/SiO_2 nanoparticles exhibited different collapse modes depending on the amphiphilicity of the Janus particle.[61]

In addition to experiments there have also been extensive theoretical studies examining the assembly behavior of various Janus particle systems.[62] In several works by Park et al., the interfacial behavior of the particles was simulated as a function of Janus particle shape, size, configuration, and amphiphilicity.[63–65] It was found that each of these characteristics plays an important role in the assembly behavior of the Janus particles. In addition, they also noted that the Janus particles could assume multiple configurations at an interface. In the work of Gao et al. the effects of Janus particle shape and size were simulated with the Janus boundary on the long axis of the anisotropic particles.[66] They found that the amphiphilicity and shape of the Janus particles have a strong impact on Janus particle interfacial behavior. Additionally, the simulated

interfacial tensions for various systems were calculated and it was found that Janus particles with complex shapes could exhibit complex adsorption kinetics with multiple assembly relaxations. These complex adsorption kinetics have been observed experimentally for shape anisotropic Janus particles.[67,68] In work by Xie et al. it was shown that the assembly structure of magnetically susceptible amphiphilic Janus particles could easily be manipulated using external magnetic fields.[69] This allowed one to tune the packing of the particles when assembled at the interface and in a final dried particle film post solvent evaporation. In all these studies, each of the systems probed both theoretically and experimentally contains a perfect Janus configuration where the particle is cleanly split into two halves of differing chemistry. There has been far less attention paid to amphiphilic Janus particles whose hydrophobic and hydrophilic domains are anisotropically distributed over the surface of the particle. The anisotropic distribution of the hydrophobic and hydrophilic domains could cause complex adsorption behavior of Janus particles similar to inducing shape anisotropy.

In this work, we employ dynamic pendant drop tensiometry to probe the interfacial assembly behavior of amphiphilic pH responsive Janus particles at a water/toluene interface. The dynamic interfacial tension (IFT) is probed as a function of particle concentration, morphology, and NaOH and HCl concentration. These experiments are then used to elucidate both the equilibrium assembly behavior of the particles, and the kinetics of their assembly. Both were found to be tunable using the particle chemistry and morphology, as well as the solution conditions.

Results and Discussion

Four categories of Janus particles were prepared using SEP and either SAPS, ACH, or a combination of both post-synthetic methods (Figure 1a). Dynamic pendant drop tensiometry was performed using a DataPhysics OCA 15plus where a video of an aqueous drop of particle solution suspended in a toluene phase was recorded. Frame-by-frame video analysis of the drop shape was then used to calculate the dynamic interfacial tension of the system as a function of time (Figure 1b).

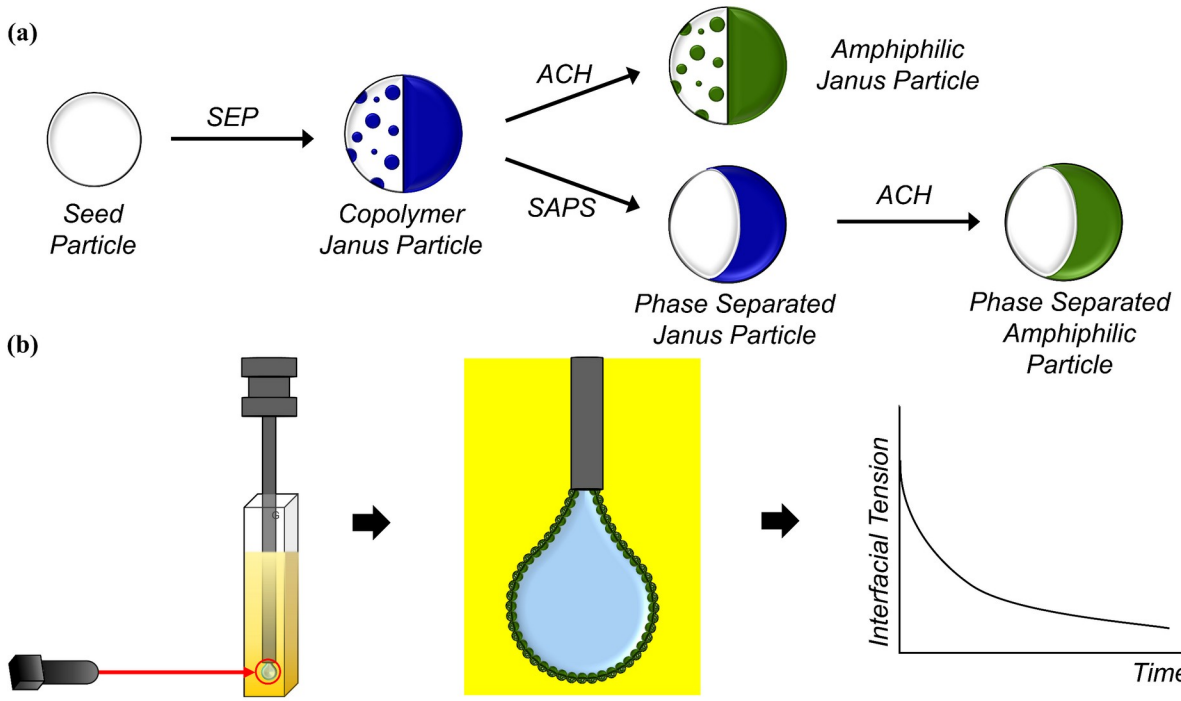

Fig. 1 a) Synthetic scheme showing the preparation of the various Janus particles synthesized for use in this study using SEP and various post-synthetic modification techniques. b) Diagram depicting the characterization of the interfacial behavior of our Janus particle systems using dynamic pendant drop tensiometry.

Synthesis and Modification of Janus Particles

A detailed description of the synthetic steps can be found in the supplemental information. Briefly, in the first step of the Janus particle synthesis polystyrene seeds for SEP were synthesized using techniques outlined by Okubo et al.[50] This synthesis yielded polystyrene seeds 476 nm in diameter, as measured by dynamic light scattering (DLS), with a PDI of 0.03 (Figure S1(a)). Infrared (IR) spectroscopy confirms the successful polymerization of the styrene monomer where the characteristic absorption peaks for polystyrene are present in the spectra (Figure S1(b)). From the SEM images in Figure 2(a) the polystyrene seeds are near monodisperse and spherical. These seeds were then swollen with a monomer feed in a seeded emulsion droplet stabilized by a 1 wt% poly(acrylic acid) solution. The monomer feed contains a 50/50 comonomer mixture of styrene and tert-butyl acrylate, a small amount of divinylbenzene as a crosslinking agent, and an azo-initiator. The crosslinking agent is added to prevent the dissolution of the polymerized copolymer phase after modification into a hydrophilic copolymer

using ACH. Upon initiation, the monomer feed inside the swollen seeded emulsion droplet begins to polymerize. The polymerization of the monomer feed triggers a copolymerization-induced phase separation producing chemically and morphologically anisotropic Janus particles. The size of the resultant Janus particles was measured using dynamic light scattering and was found to be 764 nm with a PDI of 0.02 (Figure S1(a)). This is comparable to previous reports using similar protocols to produce Janus particles approximately double in size.[52–55] From the SEM images, one can see that the Janus particles obtained from SEP contain two distinct domains of polystyrene and poly(styrene-co-tert-butyl acrylate) (Figure 2b). This is further confirmed using IR spectroscopy where one can see the absorption peaks characteristic of both the aromatic and the tert-butyl ester groups (Figure S1(b)). These particles are referred to as copolymer Janus particles (CJP).

Post-synthesis of CJPs, one can perform either ACH or SAPS to modify the CJPs chemically or morphologically. Following procedures described previously by other authors, ACH was performed on the tert-butyl ester group in the acrylate copolymer domain.[53,55] This process turns the copolymer domain of the CJPs into a hydrophilic, pH responsive domain, making the CJPs strongly amphiphilic and pH sensitive. Post-ACH the particle size, as measured by dynamic light scattering, is 703 nm with a PDI of 0.08 (Figure S1(a)). The slight decrease in size is likely due to a small loss of the copolymer phase since not all the copolymer chains are crosslinked. The increase in PDI can be attributed to an uneven swelling of the copolymer phase, since the CJPs are now amphiphilic and easily swollen with water. From the SEM images, one can see the distinct difference between these Janus particles and the CJPs (Figure 2(c)). The contrast between the polystyrene domain and the copolymer domain becomes much more distinct and the copolymer domain appears collapsed. The collapse of the copolymer domain occurs due to the loss of water under the high vacuum conditions of SEM. Further confirmation of chemical transformation is done using IR spectroscopy where the aromatic resonance peak is evident, but the tert-butyl peaks have been replaced with peaks characteristic for acrylic acid (Figure S1(b)). The Janus particles produced by doing SEP and subsequent hydrolysis (ACH) are referred to as amphiphilic Janus particles (AJP).

In the initial SEP synthesis, the morphology is a kinetically trapped non-equilibrium morphology.[53,54] As the molecular weight of the copolymer phase increases and the amount of

monomer in the seeded emulsion droplet decreases, the mobilities of the seed and copolymer phases decrease. This significant reduction in mobility arrests copolymerization induced phase separation and prevents the particle from attaining its thermodynamic equilibrium morphology. SAPS can be performed to impart mobility to the system, allowing the two phases to separate further to their equilibrium state.[53] ACH can be performed post-SAPS to yield a particle that is also amphiphilic. After doing both SAPS and a combination of SAPS and ACH, the particle sizes were measured by DLS and found to be 522 and 559 with PDIs of 0.21 and 0.01 (Figure S1(a)). From the SEM images in Figure 2(d) and 2(e) it is evident that the morphology is significantly less patchy with a more regular phase separation. This becomes clearer with the combination of SAPS and ACH as the contrast between the two domains is more evident, as with the CJPs and AJPs. IR spectroscopy confirmed that no chemical transformation occurred after performing SAPS on the CJPs. Changes in the IR spectrum were only observed after ACH was performed on the morphologically transformed Janus particles (Figure S1(b)). Janus particles produced by SEP followed by SAPS are referred to as phase-separated Janus particles (PSJP). PSJPs that were hydrolyzed using ACH are referred to as phase-separated amphiphilic particles (PSAP).

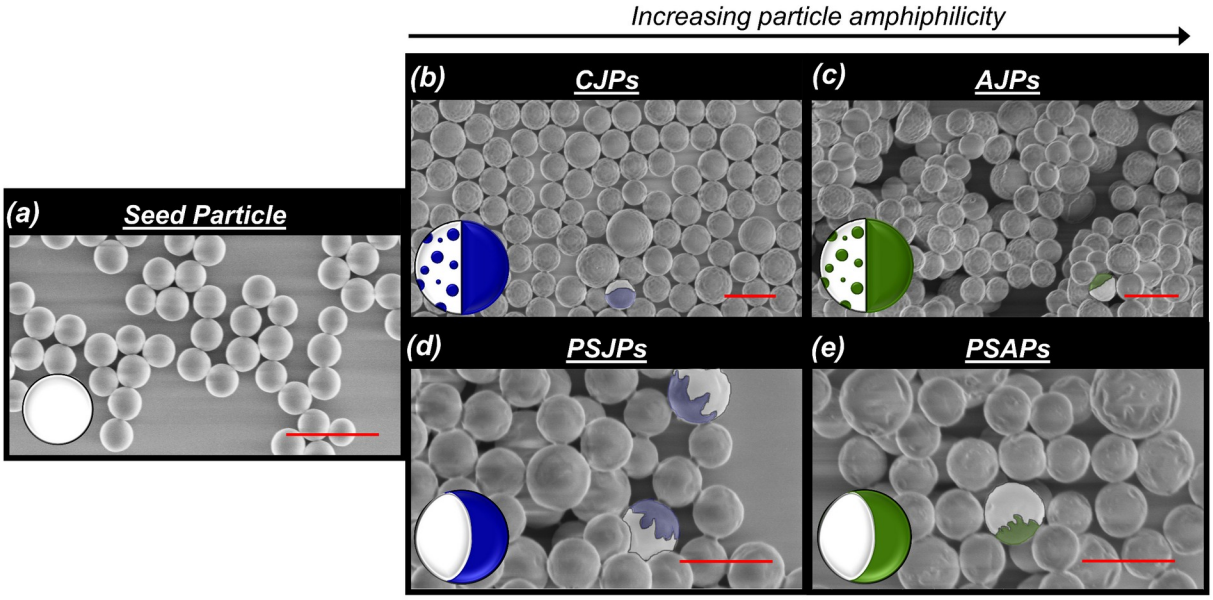

Fig. 2 SEM micrographs of the synthesized (a) polystyrene seed particles, (b) copolymer Janus particles, (c) amphiphilic Janus particles, (d) phase separated Janus particles, and (e) phase separated amphiphilic particles. Scale bars represent 1 μm. Selected Janus particles in the

micrographs have been artificially colorized to highlight the phase separation of the Janus particles.

Interfacial Behavior of Janus Particles

Previous reports of Janus particles synthesized using similar synthetic methods resulted in larger particle sizes that showed strong interfacial activity. This high interfacial activity allowed these Janus particles to be used as pH responsive solid surfactants.[55,57] To confirm that reducing the particle size by half did not affect the interfacial activity, the emulsification experiments from Tu et al. were repeated using our smaller sized AJPs (Figure S2).[62] Like their results, we found that our AJPs strongly segregate to the O/W interface to form stable Pickering emulsions. Additionally, a similar phase inversion under highly basic conditions from a W/O emulsion to an O/W emulsion was observed. These emulsions were similarly found to be stable for several months after mixing, giving us confidence that our Janus particles would show a similar degree of interfacial activity.

The IFT as a function of AJP concentration at neutral conditions was quantified using dynamic pendant drop tensiometry. Pendant drop experiments are conducted over a constant time frame of one-thousand minutes with data points collected once every five seconds. The calculated IFT is then plotted as a function of aging time to observe the time dependence of interfacial tension between the bulk toluene phase and aqueous droplet phase. As particle concentration increases one can qualitatively see that the decrease in interfacial tension is initially constant and then begins to steadily decrease (Figure S5). The IFT was then plotted a function of the log aging time to see if any complex adsorption behavior can be observed. At concentrations below 5 mg/mL one observes a single relaxation in the interfacial tension as a function of time (Figure 3(a)). This decay corresponds to the adsorption of the AJPs to the interface to reduce the interfacial tension between the aqueous and toluene phases. At concentrations higher than 5 mg/mL one observes two relaxations in the interfacial tension as a function of time (Figure 3(b)). The first decay corresponds to the AJPs initial adsorption to the interface to reduce the interfacial tension. We hypothesize the second decay at longer times arises from a reorganization of the particles at the interface. This occurs at higher concentrations because the interface is now sufficiently saturated that no other particles can absorb to the

interface to reduce the interfacial tension. Therefore, the system further reduces the interfacial tension by optimizing the particle packing and orientation at the interface.

To quantitatively understand this relaxation behavior and the time scales associated with the relaxations, the data were fit with a sum of linear exponential decays. The dynamic interfacial tension as a function of time can be expressed as,[70,71]

$$\gamma(t) = \gamma_{min} + \sum_{i=1}^{N} A_i e^{\frac{-t}{\tau_i}} \quad (2)$$

where γ_{min} is the lowest IFT achieved over a one-thousand-minute time frame, A_i is the amplitude of the decay function which is equal to the total IFT drop of the i^{th} decay function, τ_i is the relaxation time of the i^{th} decay, and N is a value varying from 1-3 depending on the total number of visible decays in the dynamic IFT. If the data are not fit with equation (2) a value for γ_{min} can be obtained by taking the average of the last 20 minutes of data recorded in $\gamma(t)$. All fit results obtained from fits of dynamic IFT concentration series data can be found in table S3 in the SI. At AJP concentrations below 5 mg/mL, data could be fit to equation (2) when N=1 since only a single exponential decay was observed in our dynamic IFT data. Fitting the data obtained at 2.5 mg/mL, we find that A_{ads} is 6.20±0.01 mN/m and τ_{ads} is 47.0±0.1 minutes. Where τ_{ads} is the relaxation time associated with AJP adsorption to the interface. At AJP concentrations above 5 mg/mL, data could be fit to equation (2) when N=2 due to the appearance of the second exponential decay in the dynamic IFT data. Fitting the data obtained at 10 mg/mL, fit values of A_{ads} and A_{recon} were calculated to be 9.54±0.02 mN/m and 7.67±0.02 mN/m while τ_{ads} and τ_{recon} are 56.1±0.1 minutes and 664±9 minutes. Where τ_{recon} is the relaxation time associated with AJP reconfiguration at the interface. From these fit values we can see that the initial adsorption of the AJPs to the interface is quite rapid while the timescale for reconfiguration is an order of magnitude longer.

This reconfiguration is predominantly governed by the rotation of the AJPs at the interface to maximize the amount that each domain is in its preferred fluid phase. If these timescales were purely due to Brownian rotation and were not influenced by any other factors, then a timescale for reconfiguration and reorientation could be estimated by $\tau_R = \frac{8\pi\eta R^3}{k_b T}$.

Jalilvand et al. estimated the diffusion coefficients for Janus micromotors at water/toluene interfaces using an effective viscosity approach.[72] An effective viscosity can be calculated by simply taking an average of the relaxation times for the Janus particle rotational diffusion coefficient where the particle is dispersed in each solvent. From this we calculate τ_R in water to be 0.268s and in toluene it is 0.150s. By taking the average of these two timescales we obtain the effective Brownian reorientation time with no interactions or contributions from interfacial tension to be 0.209s. This is many orders of magnitude faster than our measured reorientation time. However, these calculations do not consider any resistance to rotation due to the interfacial tension or the amphiphilicity of the Janus particles. Previous studies have shown that the rotation of Janus particles at interfaces can be significantly slowed as a function of particle amphiphilicity and the interfacial tension of the system.[73–76] In some cases, this gives rise to rotational relaxation times that are in the same order of magnitude as our measurements or even slower. In general, the higher the system interfacial tension and the higher the particle amphiphilicity is, the slower the reorganization of the particle at the interface are. The high degree of amphiphilicity and the uneven distribution of the hydrophilic domains on the surface of our particles strongly contributes to this slow rotational motion.

The importance of this secondary relaxation in the IFT can be seen in the fit values for γ_{min}. Fit values for γ_{min} as a function of particle concentration are plotted in figure 3(c). At concentrations lower than 5 mg/mL, the drop in γ_{min} due to the adsorption of the AJPs to the interface is approximately constant. As the concentration increases past 5 mg/mL, and particle reorganization begins to occur, one can see that the γ_{min} continually decreases with increasing concentration. This reduction is maximized at the highest concentration of 10 mg/mL where γ_{min} is almost half the value obtained at 5 mg/mL emphasizing the importance of this reorganization at the interface.

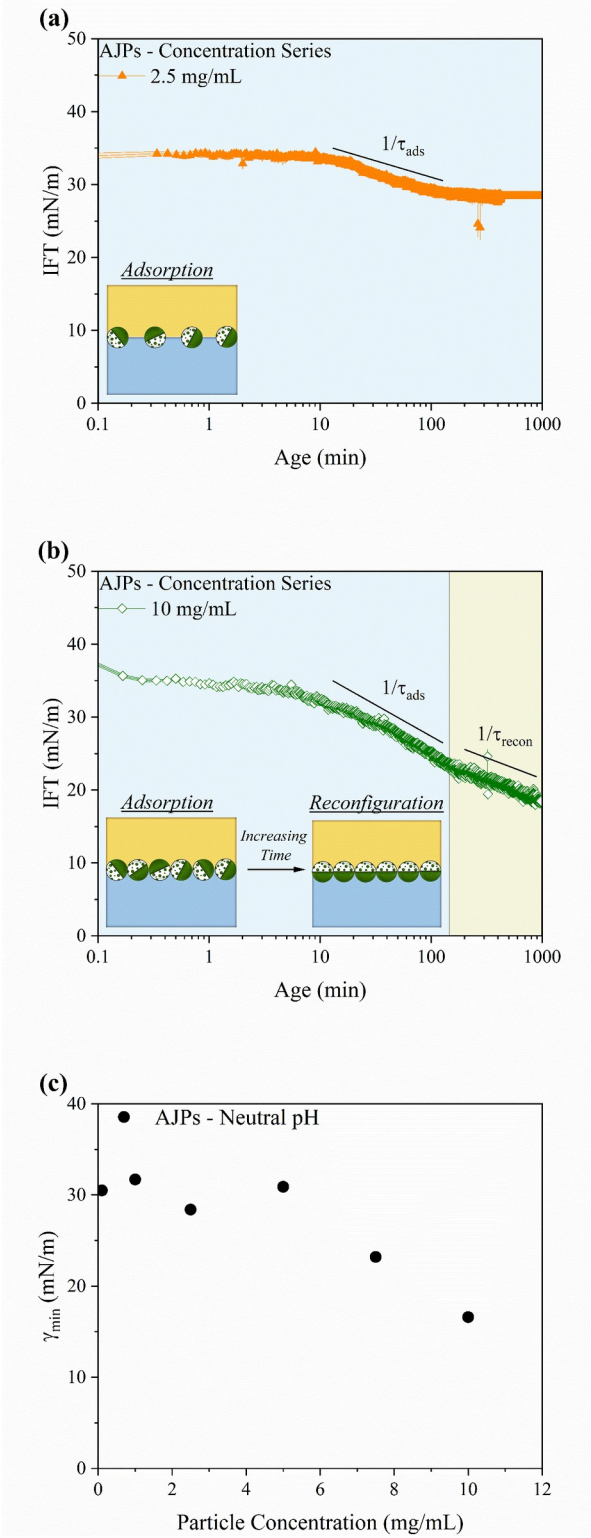

Fig. 3 Dynamic pendant drop characterization of AJPs as a function of particle concentration. Plots report the dynamic interfacial tension as a function of log-aging time for particle concentrations of (a) 2.5 and (b) 10 mg/mL. The curves are then fit with equation (2) to obtain a plot of (c) γ_{min} as a function of particle concentration.

From the previous measurements it was found that the optimal particle concentration to obtain the lowest value for γ_{min} was 10 mg/mL. Experiments were then performed to elucidate the effects of particle amphiphilicity and morphology on the Janus particles' interfacial assembly behavior. The dynamic IFT of aqueous droplets containing Janus particles of varying amphiphilicities and morphologies at a constant concentration of 10 mg/mL and neutral conditions was measured. Plots of the IFT as a function of the aging time for various synthesized particles all show complex interfacial relaxation behavior (Figure S6) that could be described using Eq. (2). It is evident from the IFT curves that the ACH Janus particles which have been made amphiphilic from ACH reduce the IFT significantly more than non-chemically modified particles. From inspection of the dynamic IFT, non-chemically modified particles can be described with only one exponential decay, while the chemically modified ones require two exponential decays. One hypothesis for the appearance of this secondary relaxation is that one of the lobes of the particles swells upon exposure to the toluene interface. However, DLS experiments where our AJPs were dispersed and allowed to equilibrate in toluene show minimal changes in the particle size (Figure S3). Additionally, if the appearance of the secondary relaxation was due to the swelling of the polystyrene phase this relaxation would appear for all Janus particles tested, not just the AJPs and PSAPs. Another alternative hypothesis for the appearance of the secondary relaxation is that the AJPs and PSAPs are undergoing an interfacial reconfiguration while the CJPs and PSJPs are not. Our data suggests that Janus particles that are not strongly amphiphilic will not undergo an interfacial relaxation to reconfigure the Janus particles into an optimal configuration and will simply adsorb to the interface. This occurs because the non-chemically modified Janus particles contain a low degree of amphiphilicity, and each domain does not have a preferential fluid phase. Whereas the Janus particles which have been chemically modified are highly amphiphilic and each domain does have a preferential fluid phase. Therefore, the system will undergo reorganization and reorientation at the water/toluene interface to put each domain in its preferred fluid phase and further reduce the systems dynamic IFT. Results from fits of the dynamic IFT of the morphology series data can be found in table S4 in the SI. Fitting the curves for the CJPs and PSJPs with equation (2) when N=1, one can see that the value for γ_{min} is approximately the same at 27.7±0.1 mN/m and 27.9±0.1 mN/m (Figure 4(a)). However, τ_{ads} differs significantly for the CJPs and PSJPs at values of 89.9±0.4 min. and

26.7±0.5 min (Figure 4(b). This suggests that morphologically modifying the particles changes the kinetics of the Janus particle assembly but not γ_{min}. For AJPs and PSAPs the fit values for γ_{min} are similar, at 16.6±0.1 mN/m and 13.4±0.2 mN/m. γ_{min} values for AJPs and PSAPs are approximately half those for the CJPs and PSJPs. In addition, a reduction in the value of τ_{ads} due to morphological modification can be observed with AJPs and PSAPs from 56.1±0.3 min. to 12.2±0.3 min. From this we can conclude that to change γ_{min} for the Janus particle systems, a chemical modification is required to make the system more amphiphilic. However, one can tune the kinetics of the adsorption process simply by tuning the particle morphology while not affecting the final value of γ_{min}.

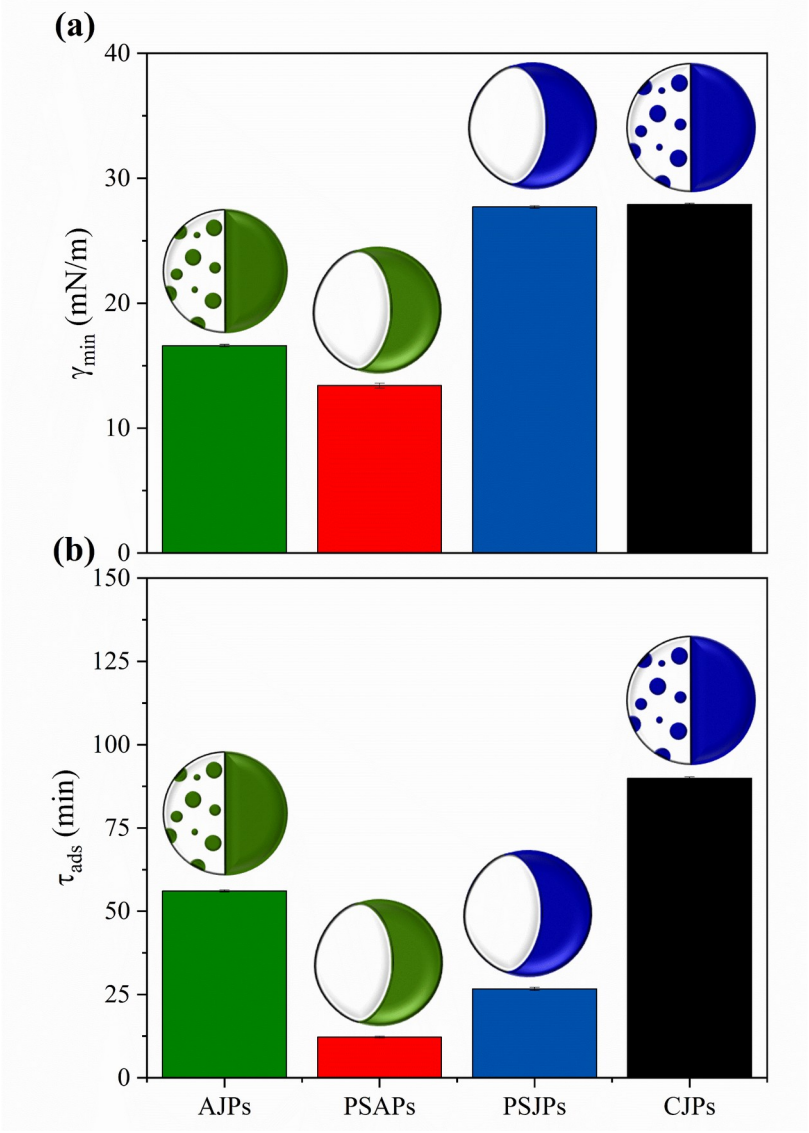

Fig. 4 – Dynamic pendant drop characterization of Janus particles of varying morphology at a concentration 10 mg/mL at neutral conditions. Plots report fit values for (a) γ_{min} and (b) τ_{ads} as a function of Janus particle morphology and amphiphilicity.

Because similar Janus particles have shown a pH-dependent behavior, it is expected that the addition of acid or base to the aqueous droplet phase will change the interfacial assembly behavior. We anticipate that varying the morphology will also influence the acid and base response of the Janus particles and yield different interfacial behavior. Dynamic IFT experiments were performed with AJPs and PSAPs dispersed in a 0.2M NaOH (aq) solution. Compared to measurements performed at neutral conditions, the equilibrium value for IFT is noticeably lower (Figure 5(a)). In addition, a third exponential decay is seen at short times in the dynamic IFT. We propose that the third relaxation corresponds to a barrier diffusion and reduced particle adsorption to the interface. Under highly basic conditions, the acrylic acid groups present in the copolymer domains become deprotonated and one portion of the particle becomes highly negatively charged. Previous studies have shown that an O/W interface generally carries a negative charge.[77–91] The two like charges create a strong enough electrostatic repulsion to slow down the adsorption of a particle to the interface. However, this force is relatively weak, and the Janus particles can eventually adsorb overcoming the electrostatic barrier. Results from fits of the dynamic IFT for the basic morphology series can be found in table S5 in the SI. The dynamic IFT data under basic conditions for AJPs and PSAPs were fit to three exponentials. Like at neutral pH, the final values for γ_{min} are quite similar at 9.52±0.01 and 11.8± 0.1, suggesting that the final equilibrium configuration of the particles is similar (Figure 5(b)). The values for $\tau_{¿¿}$ for both the AJPs and PSAPs are 0.73±0.01 min. and 0.17±0.01 min. further supporting the argument that morphological rearrangements increase the kinetics of these processes. This is even more evident when comparing values for τ_{ads} and τ_{recon} of 25.5±0.1 min. and 319±1 min, for AJPs, 20.2±0.2 min. and 195±1 min, for PSAPs (Figure 5(c)). These results show that the addition of base can affect the mechanism, kinetics, and equilibrium organization of the Janus particles at the interface. The same trends observed previously upon tuning Janus particle morphology are also observed at a different base concentration.

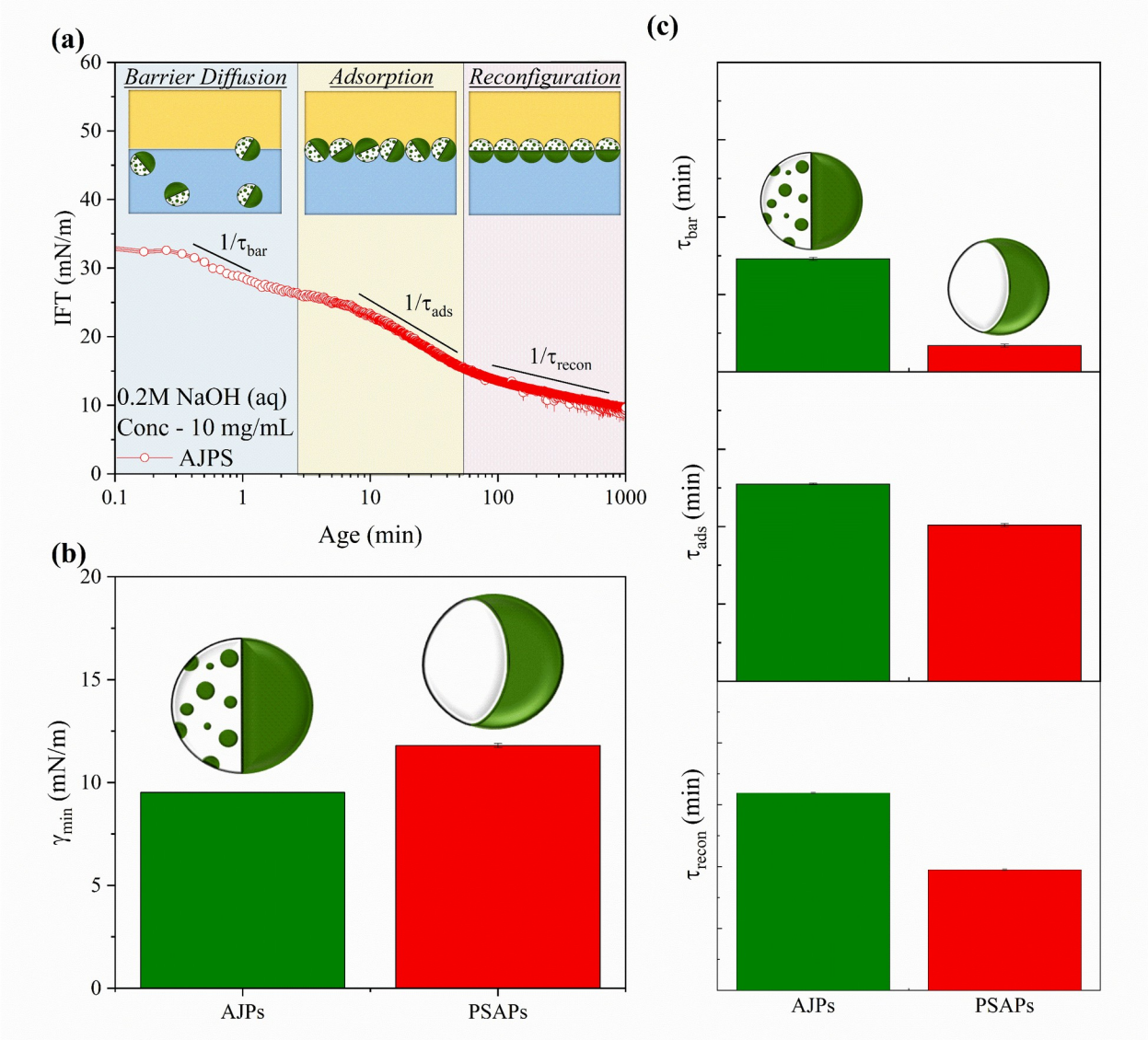

Fig. 5 - Dynamic pendant drop characterization of AJPS and PSAPs at a concentration 10 mg/mL in 0.2M NaOH (aq) solution. Plots report the dynamic IFT as a function of (a) log-aging time, (b) γ_{min}, and (c) $\tau_{¿¿}$, τ_{ads} , and τ_{recon} as a function of morphology.

Knowing that the adsorption both AJPs and PSAPs are strongly affected by pH, experiments were conducted to probe the influence of HCl and NaOH concentration on the interfacial behavior of AJPs. 10 mg/mL solutions of AJPs were prepared with 0.01M, 0.1M, and 0.2M HCl and NaOH as the continuous phase. Zeta potential measurements were performed to show that increasing the acid and base concentration in solution causes changes in the particle surface charge (Table S1 and S2). This indicates that any changes in interfacial behavior observed can most likely be attributed to the changes in the solution environment in which the

AJPs are dispersed. Upon changing the concentration of NaOH (aq) one sees quite different assembly behavior (Figure S7(a)). At a 0.01M NaOH concentration, the dynamic IFT initially decreases to ~23 mN/m but then begins to steadily increase to ~26 mN/m, then decreases again back to ~23 mN/m. Increases in IFT for charged particle systems adsorbing to oil/water interfaces has been previously observed and reported by other groups.[92–94] We hypothesize that this initial increase in the IFT is due to local distortions of the water/toluene interface by the AJPs adsorbed to the interface. The distortions occur due to increases in the magnitude of dipolar repulsions brought about the small addition of NaOH to the system. These repulsions between particles adsorbed at the interface could cause local distortions and deformations of the interface, corresponding to increases in IFT, to accommodate the further adsorption of more particles. For all other samples as the concentration of NaOH increases, γ_{min} qualitatively decreases, indicating a higher degree of interfacial activity. Results from fits of the dynamic IFT for the NaOH and HCl concentration series can be found in table S6 and S7 in the SI. Fits to the IFT curves for 0.1M and 0.2M NaOH (aq) were performed while an average γ_{min} was calculated for the 0.01M solution. From these calculated values it is evident that as NaOH concentration increases, γ_{min} decreases (Figure 6(a)). This is occurring because, as the concentration of NaOH increases, more acrylic acid groups become deprotonated and the AJPs become more amphiphilic. While this increase in amphiphilicity is simultaneously occurring, the negative charges brought about by this deprotonation are still inhibiting adsorption of the AJPs to the interface as discussed previously. This initial adsorption of our charged particles to the interface is still highly unfavorable due to their repulsion by the charged interface. However, once the particles are adsorbed to the interface this initial barrier is overcome and the particles can further reduce the system's IFT. It is the presence of NaOH in our system combined with the additional thermodynamic drivers built into amphiphilic Janus particles that allow the simultaneous observation of these phenomena. This increase in amphiphilicity facilitates the further adsorption of more AJPs, improving the stability of the O/W interface and causing a larger drop in γ_{min}. This is further supported by the fact that, upon increasing NaOH concentration, the values for τ_1, τ_2, and τ_3 do not change significantly. Additionally, upon increasing HCl concentration, the dynamics of the system change significantly without affecting γ_{min} (Figure S7(b) and 6(b)). Fitting the data to equation (2) when N=2, both τ_{ads} and τ_{recon} decrease with increasing HCl

concentration while γ_{min} fluctuates around an average value (Figure 6(c)). This is an effect of the higher counterion concentration in the aqueous phase decreasing the barrier for adsorption at higher HCl concentration. This subsequently makes it easier for particles to adsorb and assemble at the interface and increases the kinetics of their assembly without affecting their final configuration.

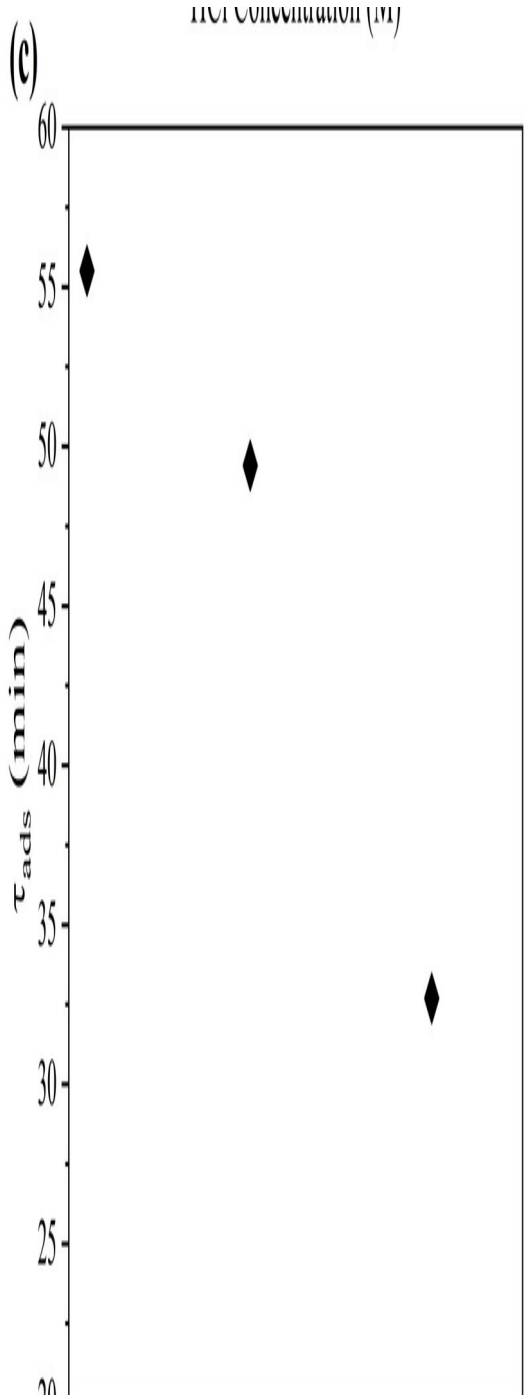

Fig. 6 - Dynamic pendant drop characterization of AJPs at a concentration 10 mg/mL in 0.01M, 0.1M, and 0.2M NaOH(aq) and HCl (aq) solutions. For AJPs under basic conditions, plots report (a) γ_{min} obtained from fits of the dynamic IFT as a function of NaOH concentration. For AJPs under acidic conditions, plots report (b) γ_{min} and (c) τ_{ads} obtained from fits of the dynamic IFT as a function of HCl concentration.

Conclusion

In this work, we synthesized and modified various classes of amphiphilic and non-amphiphilic Janus particles. Upon investigating their interfacial assembly behavior, it was found that both chemical and morphological modification were important to the final equilibrium assembly and the kinetics of assembly. By chemically modifying the Janus particles to make them more amphiphilic, the interfacial activity of the particles increased, in comparison to their non-amphiphilic counterparts. It was found that amphiphilic Janus particles could reduce the IFT by initially adsorbing to the O/W interface, and then further reduce the IFT by reorienting themselves into a more optimal configuration and packing. By morphologically modifying the particles, the final equilibrium configuration of the assembly does not change, but the kinetics of the assembly changes. Upon the addition of either acid or base to the aqueous phase, the assembly behavior could also be quite drastically altered. When adding base, a third dynamic event was found corresponding to the barrier diffusion of the Janus particles to the interface. We demonstrated that the morphology of the particles had little effect on the final equilibrium configuration when base was added to the system. Only a change in the kinetics was found due to a change in the Janus particle morphology. With the addition of acid to the system, the final equilibrium configuration did not change drastically. However, the presence of counterions in the system allowed the particles to adsorb to the interface more easily leading to faster adsorption kinetics. The use of dynamic pendant drop tensiometry has allowed us to study in detail the interfacial adsorption behavior of a large class of Janus particles. Furthermore, the analysis presented in this work has revealed aspects of amphiphilic Janus particle design that can help inform the direction of future particle syntheses for specific applications.

Conflicts of Interest

The authors have no conflicts of interest to declare.

Data Availability Statement

The data that support the findings of this study are available from the corresponding author upon reasonable request.

Acknowledgements

This work was supported by a 3M Non-tenured Faculty Award and funds from the University of Massachusetts Amherst. Additional support is provided by the U.S. Department of Energy, Office of Science, Office of Basic Energy Sciences, Materials Sciences and Engineering Division under Contract No. DE-AC02-05-CH11231 within the Adaptive Interfacial Assemblies Towards Structuring Liquids program (KCTR16) and by the National Science Foundation in contract DMR-2104883.

Supporting Information

Methods and materials for the preparation of all Janus particles and their characterization by SEM, DLS, IR spectroscopy, and dynamic pendant drop tensiometry; results and discussion of DLS and IR spectroscopy data; results from Pickering emulsion experiments with AJPs; additional results from dynamic pendant drop tensiometry experiments.

References

1. Forth, J. *et al.* Building Reconfigurable Devices Using Complex Liquid–Fluid Interfaces. *Advanced Materials* **31**, 1806370 (2019).
2. Shi, S. & Russell, T. P. Nanoparticle Assembly at Liquid–Liquid Interfaces: From the Nanoscale to Mesoscale. *Advanced Materials* vol. 30 Preprint at https://doi.org/10.1002/adma.201800714 (2018).
3. Ramsden, W. Separation of solids in the surface-layers of solutions and 'suspensions' (observations on surface-membranes, bubbles, emulsions, and mechanical coagulation).—Preliminary account. *Proceedings of the Royal Society of London* **72**, 156–164 (1904).
4. Pickering, S. U. CXCVI.—Emulsions. *J. Chem. Soc., Trans.* **91**, 2001–2021 (1907).
5. Berton-Carabin, C. C. & Schroën, K. Pickering emulsions for food applications: Background, trends, and challenges. *Annual Review of Food Science and Technology* vol. 6 263–297 Preprint at https://doi.org/10.1146/annurev-food-081114-110822 (2015).
6. Wu, J. & Ma, G. H. Recent Studies of Pickering Emulsions: Particles Make the Difference. *Small (Weinheim an der Bergstrasse, Germany)* vol. 12 4633–4648 Preprint at https://doi.org/10.1002/smll.201600877 (2016).
7. Gonzalez Ortiz, D., Pochat-Bohatier, C., Cambedouzou, J., Bechelany, M. & Miele, P. Current Trends in Pickering Emulsions: Particle Morphology and Applications. *Engineering* vol. 6 468–482 Preprint at https://doi.org/10.1016/j.eng.2019.08.017 (2020).

8. Low, L. E., Siva, S. P., Ho, Y. K., Chan, E. S. & Tey, B. T. Recent advances of characterization techniques for the formation, physical properties and stability of Pickering emulsion. *Advances in Colloid and Interface Science* vol. 277 Preprint at https://doi.org/10.1016/j.cis.2020.102117 (2020).

9. Thompson, K. L. *et al.* Covalently cross-linked colloidosomes. *Macromolecules* **43**, 10466–10474 (2010).

10. Thompson, K. L., Williams, M. & Armes, S. P. Colloidosomes: Synthesis, properties and applications. *J Colloid Interface Sci* **447**, 217–228 (2014).

11. Rossier-Miranda, F. J., Schroën, C. G. P. H. & Boom, R. M. Colloidosomes: Versatile microcapsules in perspective. *Colloids Surf A Physicochem Eng Asp* **343**, 43–49 (2009).

12. Dinsmore, A. D. *et al. Colloidosomes: Selectively Permeable Capsules Composed of Colloidal Particles*. www.sciencemag.org.

13. Huang, J. & Yang, H. A pH-switched Pickering emulsion catalytic system: High reaction efficiency and facile catalyst recycling. *Chemical Communications* **51**, 7333–7336 (2015).

14. Yang, H., Fu, L., Wei, L., Liang, J. & Binks, B. P. Compartmentalization of incompatible reagents within Pickering emulsion droplets for one-pot cascade reactions. *J Am Chem Soc* **137**, 1362–1371 (2015).

15. Chen, H., Zou, H., Hao, Y. & Yang, H. Flow Pickering Emulsion Interfaces Enhance Catalysis Efficiency and Selectivity for Cyclization of Citronellal. *ChemSusChem* **10**, 1989–1995 (2017).

16. Yang, H., Zhou, T. & Zhang, W. A strategy for separating and recycling solid catalysts based on the pH-triggered pickering-emulsion inversion. *Angewandte Chemie - International Edition* **52**, 7455–7459 (2013).

17. Zhang, M. *et al.* Compartmentalized Droplets for Continuous Flow Liquid-Liquid Interface Catalysis. *J Am Chem Soc* **138**, 10173–10183 (2016).

18. Seo, B., Sung, M., Park, B. J. & Kim, J. W. Recyclable 2D Colloid Surfactants with High Catalytic Activities at Pickering Emulsion Interfaces. *Adv Funct Mater* **32**, (2022).

19. Lu, T., Gou, H., Rao, H. & Zhao, G. Recent progress in nanoclay-based Pickering emulsion and applications. *Journal of Environmental Chemical Engineering* vol. 9 Preprint at https://doi.org/10.1016/j.jece.2021.105941 (2021).

20. Zhao, X., He, F., Yu, G., Feng, Y. & Li, J. High-viscosity Pickering emulsion stabilized by amphiphilic alginate/SiO2 via multiscale methodology for crude oil-spill remediation. *Carbohydr Polym* **273**, (2021).

21. Zhang, W. *et al.* Bifunctional remediation of oil spills based on pickering emulsification of polypyrrole-Ag3PO4/AgCl@Palygorskite. *Sep Purif Technol* **301**, (2022).

22. Panchal, A. *et al.* Bacterial proliferation on clay nanotube Pickering emulsions for oil spill bioremediation. *Colloids Surf B Biointerfaces* **164**, 27–33 (2018).

23. Lee, J. G., Larive, L. L., Valsaraj, K. T. & Bharti, B. Binding of Lignin Nanoparticles at Oil-Water Interfaces: An Ecofriendly Alternative to Oil Spill Recovery. *ACS Appl Mater Interfaces* **10**, 43282–43289 (2018).

24. Qiu, B. *et al.* Interfacially Super-Assembled Asymmetric and H2O2 Sensitive Multilayer-Sandwich Magnetic Mesoporous Silica Nanomotors for Detecting and Removing Heavy Metal Ions. *Adv Funct Mater* **31**, (2021).

25. Hu, Y., Liu, W. & Sun, Y. Self-Propelled Micro-/Nanomotors as "On-the-Move" Platforms: Cleaners, Sensors, and Reactors. *Advanced Functional Materials* vol. 32 Preprint at https://doi.org/10.1002/adfm.202109181 (2022).

26. Cain, J. D. *et al.* Sculpting Liquids with Two-Dimensional Materials: The Assembly of Ti3C2Tx MXene Sheets at Liquid-Liquid Interfaces. *ACS Nano* **13**, 12385–12392 (2019).

27. Shi, S. *et al.* Self‐Assembly of MXene‐Surfactants at Liquid–Liquid Interfaces: From Structured Liquids to 3D Aerogels. *Angewandte Chemie* **131**, 18339–18344 (2019).

28. Yan, J. *et al.* Structured-Liquid Batteries. *J Am Chem Soc* **144**, 3979–3988 (2022).

29. Popple, D. *et al.* All‐Liquid Reconfigurable Electronics Using Jammed MXene Interfaces. *Advanced Materials* 2208148 (2022) doi:10.1002/adma.202208148.

30. Binks, B. P. Particles as surfactants—similarities and differences. *Curr Opin Colloid Interface Sci* **7**, 21–41 (2002).

31. Koretsky, A. & Kruglyakov, P. Emulsifying effects of solid particles and the energetics of putting them at the water-oil interface. *Izv. Sib. Otd. Akad. Nauk USSR* **2**, 139 (1971).

32. Cui, M., Emrick, T. & Russell, T. P. Stabilizing Liquid Drops in Nonequilibrium Shapes by the Interfacial Jamming of Nanoparticles. *Science (1979)* **342**, 460–463 (2013).

33. Forth, J. *et al.* Reconfigurable Printed Liquids. *Advanced Materials* **30**, (2018).

34. Huang, C. *et al.* Structured Liquids with pH-Triggered Reconfigurability. *Advanced Materials* **28**, 6612–6618 (2016).

35. Zhang, J., Grzybowski, B. A. & Granick, S. Janus Particle Synthesis, Assembly, and Application. *Langmuir* **33**, 6964–6977 (2017).

36. Safaie, N. & Ferrier, R. C. Janus nanoparticle synthesis: Overview, recent developments, and applications. *J Appl Phys* **127**, 170902 (2020).

37. Liang, F., Zhang, C. & Yang, Z. Rational design and synthesis of Janus composites. *Advanced Materials* **26**, 6944–6949 (2014).

38. Loget, G., Roche, J. & Kuhn, A. True bulk synthesis of Janus objects by bipolar electrochemistry. *Advanced Materials* **24**, 5111–5116 (2012).

39. Perro, A., Reculusa, S., Ravaine, S., Bourgeat-Lami, E. & Duguet, E. Design and synthesis of Janus micro- and nanoparticles. *J Mater Chem* **15**, 3745–3760 (2005).

40. Pawar, A. B. & Kretzschmar, I. Fabrication, assembly, and application of patchy particles. *Macromol Rapid Commun* **31**, 150–168 (2010).

41. McGlasson, A. & Bradley, L. C. Investigating Time-Dependent Active Motion of Janus Micromotors using Dynamic Light Scattering. *Small* **17**, (2021).

42. Bradley, L. C., Chen, W. H., Stebe, K. J. & Lee, D. Janus and patchy colloids at fluid interfaces. *Curr Opin Colloid Interface Sci* **30**, 25–33 (2017).

43. Kumar, A., Park, B. J., Tu, F. & Lee, D. Amphiphilic Janus particles at fluid interfaces. *Soft Matter* **9**, 6604–6617 (2013).

44. Binks, B. P. & Fletcher, P. D. I. Particles adsorbed at the oil-water interface: A theoretical comparison between spheres of uniform wettability and 'Janus' particles. *Langmuir* **17**, 4708–4710 (2001).

45. Visaveliya, N. R. & Köhler, J. M. Hierarchical Assemblies of Polymer Particles through Tailored Interfaces and Controllable Interfacial Interactions. *Adv Funct Mater* **31**, (2021).

46. Deng, R., Xu, J., Yi, G. R., Kim, J. W. & Zhu, J. Responsive Colloidal Polymer Particles with Ordered Mesostructures. *Advanced Functional Materials* vol. 31 Preprint at https://doi.org/10.1002/adfm.202008169 (2021).

47. Zhang, Y. *et al.* Single Copolymer Chain-Templated Synthesis of Ultrasmall Symmetric and Asymmetric Silica-Based Nanoparticles. *Adv Funct Mater* **32**, (2022).

48. Sudjaipraparat, N., Kaewsaneha, C., Nuasaen, S. & Tangboriboonrat, P. One-pot synthesis of non-spherical hollow latex polymeric particles via seeded emulsion polymerization. *Polymer (Guildf)* **121**, 165–172 (2017).

49. Fan, J. B. *et al.* A general strategy to synthesize chemically and topologically anisotropic Janus particles. *Sci Adv* **3**, 1–9 (2017).

50. Okubo, M., Fujiwara, T. & Yamaguchi, A. Morphology of anomalous polystyrene/ polybutyl acrylate composite particles produced by seeded emulsion polymerization. *Colloid Polym Sci* **276**, 186–189 (1998).

51. Pei, X. *et al.* Fabrication of shape-tunable macroparticles by seeded polymerization of styrene using non-cross-linked starch-based seed. *J Colloid Interface Sci* **512**, 600–608 (2018).

52. Bradley, L. C., Stebe, K. J. & Lee, D. Clickable Janus Particles. *J Am Chem Soc* **138**, 11437–11440 (2016).

53. Hamilton, H. S. C. & Bradley, L. C. Probing the morphology evolution of chemically anisotropic colloids prepared by homopolymerization- and copolymerization-induced phase separation. *Polym Chem* **11**, 230–235 (2020).

54. Chen, W.-H., Tu, F., Bradley, L. C. & Lee, D. Shape-Tunable Synthesis of Sub-Micrometer Lens-Shaped Particles via Seeded Emulsion Polymerization. *Chemistry of Materials* **29**, 2685–2688 (2017).

55. Tu, F. & Lee, D. Shape-changing and amphiphilicity-reversing Janus particles with pH-responsive surfactant properties. *J Am Chem Soc* **136**, 9999–10006 (2014).

56. Glaser, N., Adams, D. J., Böker, A. & Krausch, G. Janus Particles at Liquid−Liquid Interfaces. *Langmuir* **22**, 5227–5229 (2006).

57. Lan, Y. *et al.* Janus Particles with Varying Configurations for Emulsion Stabilization. *Ind Eng Chem Res* **58**, 20961–20968 (2019).

58. Park, B. J., Brugarolas, T. & Lee, D. Janus particles at an oil-water interface. *Soft Matter* **7**, 6413–6417 (2011).

59. Park, B. J. *et al.* Double hydrophilic janus cylinders at an air-water interface. *Langmuir* **29**, 1841–1849 (2013).

60. Razavi, S., Hernandez, L. M., Read, A., Vargas, W. L. & Kretzschmar, I. Surface tension anomaly observed for chemically-modified Janus particles at the air/water interface. *J Colloid Interface Sci* **558**, 95–99 (2019).

61. Razavi, S., Lin, B., Lee, K. Y. C., Tu, R. S. & Kretzschmar, I. Impact of Surface Amphiphilicity on the Interfacial Behavior of Janus Particle Layers under Compression. *Langmuir* **35**, 15813–15824 (2019).

62. Tu, F., Park, B. J. & Lee, D. Thermodynamically stable emulsions using Janus dumbbells as colloid surfactants. *Langmuir* **29**, 12679–12687 (2013).

63. Park, B. J. & Lee, D. Equilibrium orientation of nonspherical Janus particles at fluid-fluid interfaces. *ACS Nano* **6**, 782–790 (2012).

64. Park, B. J. & Lee, D. Configuration of nonspherical amphiphilic particles at a fluid-fluid interface. *Soft Matter* **8**, 7690–7698 (2012).

65. Park, B. J. & Lee, D. Particles at fluid-fluid interfaces: From single-particle behavior to hierarchical assembly of materials. *MRS Bull* **39**, 1089–1096 (2014).

66. Gao, H. M., Lu, Z. Y., Liu, H., Sun, Z. Y. & An, L. J. Orientation and surface activity of Janus particles at fluid-fluid interfaces. *Journal of Chemical Physics* **141**, (2014).

67. Ruhland, T. M., Gröschel, A. H., Walther, A. & Müller, A. H. E. Janus cylinders at liquid-liquid interfaces. *Langmuir* **27**, 9807–9814 (2011).

68. Ruhland, T. M. *et al.* Influence of janus particle shape on their interfacial behavior at liquid-liquid interfaces. *Langmuir* **29**, 1388–1394 (2013).

69. Xie, Q., Davies, G. B. & Harting, J. Direct Assembly of Magnetic Janus Particles at a Droplet Interface. *ACS Nano* **11**, 11232–11239 (2017).

70. Seong, H. G., Chen, Z., Emrick, T. & Russell, T. P. Reconfiguration and Reorganization of Bottlebrush Polymer Surfactants. *Angewandte Chemie - International Edition* **61**, (2022).

71. Chen, Z. *et al.* In Situ Hydrolysis of Block Copolymers at the Water-Oil Interface. *Angewandte Chemie - International Edition* **61**, (2022).

72. Jalilvand, Z., Haider, H., Cui, J. & Kretzschmar, and I. Pt-SiO 2 Janus Particles and the Water/Oil Interface: A Competition between Motility and Thermodynamics. *Langmuir* **36**, 6880–6887 (2020).

73. Stocco, A., Chollet, B., Wang, X., Blanc, C. & Nobili, M. Rotational diffusion of partially wetted colloids at fluid interfaces. *J Colloid Interface Sci* **542**, 363–369 (2019).

74. Rezvantalab, H., Drazer, G. & Shojaei-Zadeh, S. Molecular simulation of translational and rotational diffusion of Janus nanoparticles at liquid interfaces. *J Chem Phys* **142**, 014701 (2015).

75. Rezvantalab, H. & Shojaei-Zadeh, S. Tilting and Tumbling of Janus Nanoparticles at Sheared Interfaces. *ACS Nano* **10**, 5354–5361 (2016).

76. Wang, D. *et al.* Brownian Diffusion of Individual Janus Nanoparticles at Water/Oil Interfaces. *ACS Nano* **14**, 10095–10103 (2020).

77. Vácha, R. *et al.* The Orientation and Charge of Water at the Hydrophobic Oil Droplet–Water Interface. *J Am Chem Soc* **133**, 10204–10210 (2011).

78. Vazdar, M., Pluhařová, E., Mason, P. E., Vácha, R. & Jungwirth, P. Ions at Hydrophobic Aqueous Interfaces: Molecular Dynamics with Effective Polarization. *J Phys Chem Lett* **3**, 2087–2091 (2012).

79. Zangi, R. & Engberts, J. B. F. N. Physisorption of Hydroxide Ions from Aqueous Solution to a Hydrophobic Surface. *J Am Chem Soc* **127**, 2272–2276 (2005).

80. Mundy, C. J., Kuo, I.-F. W., Tuckerman, M. E., Lee, H.-S. & Tobias, D. J. Hydroxide anion at the air–water interface. *Chem Phys Lett* **481**, 2–8 (2009).

81. Kudin, K. N. & Car, R. Why Are Water–Hydrophobic Interfaces Charged? *J Am Chem Soc* **130**, 3915–3919 (2008).

82. Gray-Weale, A. & Beattie, J. K. An explanation for the charge on water's surface. *Physical Chemistry Chemical Physics* **11**, 10994 (2009).

83. Knecht, V., Risselada, H. J., Mark, A. E. & Marrink, S. J. Electrophoretic mobility does not always reflect the charge on an oil droplet. *J Colloid Interface Sci* **318**, 477–486 (2008).

84. Beattie, J. K. & Djerdjev, A. M. The Pristine Oil/Water Interface: Surfactant-Free Hydroxide-Charged Emulsions. *Angewandte Chemie International Edition* **43**, 3568–3571 (2004).

85. Dickinson, W. The effect of pH upon the electrophoretic mobility of emulsions of certain hydrocarbons and aliphatic halides. *Transactions of the Faraday Society* **37**, 140 (1941).

86. Stachurski, J. & MichaŁek, M. The Effect of the ζ Potential on the Stability of a Non-Polar Oil-in-Water Emulsion. *J Colloid Interface Sci* **184**, 433–436 (1996).

87. Creux, P., Lachaise, J., Graciaa, A., Beattie, J. K. & Djerdjev, A. M. Strong Specific Hydroxide Ion Binding at the Pristine Oil/Water and Air/Water Interfaces. *J Phys Chem B* **113**, 14146–14150 (2009).

88. Marinova, K. G. *et al.* Charging of Oil−Water Interfaces Due to Spontaneous Adsorption of Hydroxyl Ions. *Langmuir* **12**, 2045–2051 (1996).

89. Dunstan, D. E. & Saville, D. A. Electrokinetic potential of the alkane/aqueous electrolyte interface. *Journal of the Chemical Society, Faraday Transactions* **89**, 527 (1993).

90. Dunstan, D. E. & Saville, D. A. Electrophoretic mobility of colloidal alkane particles in electrolyte solutions. *Journal of the Chemical Society, Faraday Transactions* **88**, 2031 (1992).

91. Dunstan, D. E. Temperature Dependence of the Electrokinetic Properties of Two Disparate Surfaces. *J Colloid Interface Sci* **166**, 472–475 (1994).

92. Wang, W., Zhou, Z., Nandakumar, K., Xu, Z. & Masliyah, J. H. Effect of charged colloidal particles on adsorption of surfactants at oil–water interface. *J Colloid Interface Sci* **274**, 625–630 (2004).

93. Eskandar, N. G., Simovic, S. & Prestidge, C. A. Interactions of hydrophilic silica nanoparticles and classical surfactants at non-polar oil–water interface. *J Colloid Interface Sci* **358**, 217–225 (2011).

94. Bergfreund, J., Sun, Q., Fischer, P. & Bertsch, P. Adsorption of charged anisotropic nanoparticles at oil–water interfaces. *Nanoscale Adv* **1**, 4308–4312 (2019).